

1 **Pumping optimization of coastal aquifers using seawater**
2 **intrusion models of variable-fidelity and evolutionary**
3 **algorithms**

4

5 Vasileios Christelis^{1,2} and Aristotelis Mantoglou¹

6

7 ¹ Laboratory of Reclamation Works and Water Resources Management, School of
8 Rural and Surveying Engineering, National Technical University of Athens,
9 Athens, Greece

10 ² British Geological Survey, Environmental Science Centre, Keyworth,
11 Nottingham, UK

12

13 Corresponding author: Vasileios Christelis (vchrist@survey.ntua.gr)

14

15 **Abstract:**

16 Variable-fidelity modelling has been utilized in several engineering optimization
17 studies to construct surrogate models. However, similar approaches have received
18 much less attention in coastal aquifer management problems. A variable-fidelity
19 optimization framework was developed utilizing a lower-fidelity and
20 computationally cheap model of seawater intrusion, based on the sharp interface
21 assumption, and a simple correction process. The variable-fidelity method was
22 compared to the direct optimization with the high-fidelity variable density and salt
23 transport model and to conventional surrogate-based optimization. The surrogate-

24 based approaches were embedded into the operations of an evolutionary algorithm
25 to implement an efficient online update of the surrogate models and control the
26 feasibility of the optimal solutions. Multiple independent optimization runs were
27 performed to provide more insightful comparison outcomes. Although the
28 variable-fidelity method found a better optimum than the conventional approach,
29 the overall sample statistics showed that the surrogate-based optimization
30 frameworks performed equally well and provided good approximations to the
31 high-fidelity solution. Despite the potential for an improved exploration of the
32 optimal search space by using the variable-fidelity method, the conventional
33 approach had a 30% faster average convergence time.

34

35 **1. Introduction**

36 The seawater intrusion phenomenon is a common problem of coastal aquifers,
37 particularly for semi-arid areas where low recharge and increased groundwater
38 extraction threatens the sustainability of freshwater resources (Petalas et al. 2009).
39 Typically, simulation-optimization routines based on seawater intrusion models
40 and optimization algorithms, are utilized to calculate maximum groundwater
41 abstraction subject to constraints that control the landward advancement of
42 seawater (Singh 2014). Variable density and salt transport (VDST) numerical
43 models have been effectively employed in several seawater intrusion studies (e.g.
44 Kerrou et al. 2013; Mahmoodzadeh et al. 2014), however, the resulting
45 computational cost hinders their use in simulation-optimization frameworks for
46 coastal aquifer management.

47 To reduce the computational burden, recent coastal aquifer management
48 studies have used surrogate modelling techniques to emulate the response of VDST
49 models and enable a computationally tractable optimization model (Sreekanth and
50 Datta 2015). The use of surrogate modelling in the various engineering
51 optimization problems is often reported as surrogate-based optimization (SBO)
52 (Forrester and Keane 2009). Common practice is to create first a space-filling
53 design for the input data and then run the expensive computer models to obtain the
54 required quantity of interest. The surrogate models are then constructed based on
55 these input-output data (Razavi et al. 2012a). Given that the trained surrogate
56 models have attained a reasonable level of accuracy, they are used to provide fast
57 approximations of the original numerical model response to unseen data (Forrester
58 and Keane 2008). The successful construction of a surrogate model largely
59 depends on the size and the spread of the sampling design. However, it is often
60 impractical to use a large sample of input-output data from the original computer
61 models due to computational restrictions. In those cases, it is more effective and
62 efficient to update the initial surrogate model with new training points by utilizing
63 an iterative process (Regis 2011; Zhou et al. 2017).

64 Significant improvements on the computational requirements for coastal
65 aquifer management have been achieved through the application of the so-called
66 adaptive SBO frameworks (e.g. Kourakos and Mantoglou 2009; Papadopoulou et
67 al. 2010; Christelis et al. 2017; Song et al. 2018). Several surrogate modelling
68 techniques have been proposed in the coastal aquifer management literature
69 including artificial neural networks (Ataie-Ashtiani et al. 2013; Huang and Chiu
70 2018), genetic programming (Sreekanth and Datta 2011), evolutionary polynomial
71 regression (Hussain et al. 2015), Gaussian process models (Rajabi and Ketabchi

72 2017), radial basis functions (Christelis and Mantoglou 2016a), fuzzy inference
73 systems (Roy and Datta 2017a), multivariate adaptive regression splines (Roy and
74 Datta 2017b) and support vector machine regression (Lal and Data 2018).

75 Often, the exploration of the optimal search space may be informed by
76 simpler, computationally efficient models which simulate the physical system at a
77 lower-fidelity level (Forrester et al. 2008). This possibility has motivated the
78 development of variable-fidelity or multi-fidelity optimization (Robinson et al.
79 2006). Under this framework, surrogate models are constructed using faster lower
80 fidelity models which may share the same physics with the computationally
81 expensive high-fidelity models but are less accurate in terms of grid resolution,
82 convergence criteria, dimensionality, or can be conceptual simplifications of the
83 physical system (Razavi et al., 2012b; Asher et al. 2015). Numerous variable-
84 fidelity frameworks have been developed in the field of electromagnetic
85 simulations through the application of the space mapping technique (Bandler et al.
86 1994; Koziel et al. 2006), as well as, in aerospace engineering utilizing response
87 correction techniques (e.g. Alexandrov et al. 2001; Gano et al. 2004). Most of the
88 times, the variable-fidelity methods involve the construction of a surrogate model
89 which combines the available fidelity levels and corrects the less accurate but fast
90 lower-fidelity models towards the response of the high-fidelity model (Park et al.
91 2016).

92 Since lower-fidelity models utilize their embedded knowledge of the physical
93 system to produce an output, they may offer some benefits for the implementation
94 of SBO (Kennedy and O' Hagan 2000; Koziel and Leifsson 2016). That is, the
95 lower-fidelity model is capable to explain part of the high-fidelity model behavior
96 which in turn may effectively direct the SBO algorithm to promising regions. It is

97 possible though, that the differences between the lower-fidelity and the high-
98 fidelity model to be significant. In that case, the surrogate model may have to
99 approximate abrupt changes in the variable-fidelity data which can be addressed by
100 applying an informative sampling strategy (Zhou et al. 2016). It should be noted
101 that a variable-fidelity SBO may add computational effort and this must always be
102 considered as a possible drawback. Therefore, it is convenient to employ lower-
103 fidelity models which retain a certain degree of accuracy while being much faster
104 than the high-fidelity model.

105 In the case of seawater intrusion simulation, a coarse taxonomy of the fidelity
106 levels may consider VDST models as high-fidelity models. Then, seawater
107 intrusion models that neglect dispersion mechanisms but simulate saltwater
108 movement (Essaid 1986) or coastal aquifer flow with density variations (Bakker
109 2003), may represent lower levels of fidelity. An additional simplification and thus
110 an even lower-fidelity level could be defined by sharp interface models which
111 assume static seawater (Strack 1976; Mantoglou et al 2004; Koussis et al. 2012).
112 Obviously, there are other fidelity levels that could be identified in a seawater
113 intrusion simulation framework (VDST models of coarser resolution, steady-state
114 instead of transient coastal aquifer models, etc). In their recent review paper,
115 Sreekanth and Datta (2015) do not report any variable-fidelity applications
116 developed for coastal aquifer management. In the context of variable-fidelity
117 optimization for coastal aquifer management, Christelis and Mantoglou (2016b)
118 recently proposed a method which adaptively corrects the density ratio of a lower-
119 fidelity sharp interface model to adjust its response towards that of the high-fidelity
120 VDST model. Although not explicitly formulated in their work, that approach has

121 some similarities to the implicit space mapping method, but it lacks proper
122 convergence and it is mostly capable of quickly locating promising solutions.

123 Given the little investigation of variable-fidelity methods in coastal aquifer
124 management, the present work, implements such an approach for a single-objective
125 pumping optimization problem. Here, VDST numerical simulations represent the
126 high-fidelity data whereas a sharp interface model, based on the single-potential
127 formulation of Strack (1976), is employed as a lower-fidelity model. The latter is a
128 simple and computationally efficient model of seawater intrusion which has been
129 employed in several studies to develop simulation-optimization routines (e.g.
130 Mantoglou et al. 2004; Karatzas and Dokou 2015). Therefore, it is worthwhile to
131 investigate its applicability in variable-fidelity optimization frameworks for coastal
132 aquifer management. For comparison purposes, the performance of the variable-
133 fidelity optimization method is evaluated against direct optimization with the
134 VDST model and against conventional SBO with radial basis functions as
135 surrogate models. To enable a more comprehensive comparison among the
136 proposed methods, multiple independent runs of the SBO frameworks are
137 performed. To the best of authors' knowledge, this is the first study in coastal
138 aquifer management which employs a variable-fidelity optimization strategy for
139 reducing the computational cost of the VDST-based optimization and compares its
140 applicability against conventional SBO approaches.

141

142 **2. Coastal aquifer simulation and pumping optimization**

143 A brief discussion follows regarding the coastal aquifer simulation models that
144 were used in this study. The mathematical formulation of these models has been
145 extensively presented in the relevant literature and it is omitted here for brevity.

146 **2.1 The SI models**

147 VDST models emulate dispersion mechanisms and density variability in space and
148 are considered high-fidelity approximations of coastal aquifer processes (Dokou
149 and Karatzas 2012). The 3D simulations of variable density and salt transport
150 dynamics are based on numerical codes which solve a coupled system of partial
151 differential equations (Werner et al. 2013). VDST modelling is considered a
152 computationally expensive task due to the spatial and time discretization
153 requirements of the solute transport step (Werner et al. 2013). In the present paper,
154 the HydroGeoSphere numerical code (Graf and Therrien 2005) was used to
155 simulate seawater intrusion. HydroGeoSphere applies the control volume finite
156 element method with adaptive time-stepping to solve the coupled system of flow
157 and transport equations and utilizes a Picard iteration scheme to cycle between
158 them (Therrien et al. 2006). Thereinafter, the VDST model will be interchangeably
159 called high-fidelity model.

160 Sharp interface models based on Ghyben-Herzberg approximation and the
161 single-potential formulation of Strack (1976), are considered as lower-fidelity
162 models since they neglect density variability in space and mixing between
163 freshwater and saltwater. Seawater is assumed static and aquifer flow is horizontal
164 and steady-state. Thus, the dimensionality of the seawater intrusion simulation is
165 reduced to a simple 2D flow equation problem (Mantoglou et al. 2004). Several

166 comprehensive theoretical presentations of the sharp interface approximation can
 167 be found elsewhere in the literature (e.g. Strack 1976; Cheng and Quazar 1999).
 168 Here, we apply the numerical solution of the flow problem for coastal aquifers of
 169 finite size as described in Mantoglou et al. (2004). Thereinafter, the sharp interface
 170 model will be interchangeably called lower-fidelity model.

171 **2.2 Coastal aquifer model settings**

172 The numerical simulations are based on an illustrative coastal aquifer model of
 173 rectangular shape, which approximates a real aquifer at the Greek Island of
 174 Kalymnos (Mantoglou et al. 2004). The dimensions of the coastal aquifer model
 175 are $x=7000m$, $y=3000m$ while the aquifer thickness is $z=25m$. Unconfined,
 176 steady-state and saturated flow conditions are assumed and the aquifer is
 177 replenished by both recharge and lateral fluxes. Table 1 summarizes the basic input
 178 parameters for both the VDST and the sharp interface numerical models.

179 **Table 1.** Parameters for the numerical SI simulations

Model parameters	VDST (3D)	Sharp interface (2D)
$K_x, K_y, K_z (m/day)$	100,100,10	100, 100,*
$R_{gw} (m^3/day)$	5422	5422
$\alpha_L, \alpha_T (m)$	100,10	*
$\Delta_x, \Delta_y, \Delta_z (m)$	100,100,5	100,100,*

180 K_x, K_y, K_z : hydraulic conductivities, R_{gw} : total aquifer recharge, α_L, α_T : longitudinal and
181 transverse dispersivity values, $\Delta_x, \Delta_y, \Delta_z$: grid discretization settings, *: not applicable

182

183 In the absence of real-world data, the dispersivity values for the VDST model
184 were selected to facilitate the setup of a faster VDST model since spatial
185 discretization is related to the dispersivity values via the mesh Peclet number.
186 Note that due to the exploratory nature of this work, multiple runs are performed
187 for the SBO frameworks to take into account the stochastic nature of the
188 evolutionary algorithm and produce an insightful comparison output. In that sense,
189 a relatively fast VDST model is required to realize such a demanding
190 computational task. A single run of the VDST model required an approximate
191 CPU time of 30 seconds, running on a 2.53 GHz Intel i5 processor with 6 GB of
192 RAM in a 64-bit Windows 7 system. On the contrary, a single run of the sharp
193 interface model based on the same computer settings is 0.52 seconds. An initial
194 simulation run of the VDST model was performed with no pumping present, until
195 the head and salinity concentration fields reached steady-state. This step provided
196 the initial conditions for the VDST simulations related to the optimization part of
197 this study.

198 **2.3 Pumping optimization based on the SI models**

199 VDST and sharp interface models do not share the same physics and thus, they
200 differ in terms of input parameters and output variables. VDST simulations
201 provide a salinity concentration field for the calculation of seawater intrusion. On
202 the contrary, the output from the sharp interface model is a single-potential flow
203 field which is used to calculate the “toe” of interface (Mantoglou et al. 2004). The

204 formulation of the optimization problem is presented for nonlinear constraint
 205 functions considering fully penetrating pumping wells. The VDST-based
 206 optimization is mathematically defined as follows:

207

$$\begin{aligned}
 & \min - \sum_{i=1}^M Q_i \\
 208 \quad & s.t. \quad x_i^{c_{\max}}(Q_1, Q_2, \dots, Q_M) \leq xw_i, \forall i = 1, 2, \dots, M \\
 & \quad Q_{\min} \leq Q_i \leq Q_{\max}, i = 1, 2, \dots, M
 \end{aligned} \tag{1}$$

209

210 where M is the number of pumping wells, Q_i represents the individual pumping
 211 rate, xw_i is the horizontal distance of the well from the coastline, $x_i^{c_{\max}}$ is the
 212 horizontal distance of the iso-salinity line c_{\max} from the coast as a function of
 213 the pumping rates, and Q_{\min} and Q_{\max} define the lower and upper limits of
 214 pumping rates, respectively. Therefore, the problem is set as the maximization of
 215 the extracted groundwater amount by M pumping wells, subject to constraints
 216 that maintain the levels of salinity concentration in pumped groundwater up to a
 217 potable limit c_{\max} . The maximum salinity level of $c_{\max} = 35 \text{ mg/lt}$, was
 218 selected to formulate the high-fidelity constraint functions.

219

220 The corresponding optimization formulation for the sharp interface models is:

221

$$\begin{aligned}
 & \min - \sum_{i=1}^M Q_i \\
 222 \quad & s.t. \quad x_i^{toe}(Q_1, Q_2, \dots, Q_M) < xw_i, \forall i = 1, 2, \dots, M \\
 & \quad Q_{\min} \leq Q_i \leq Q_{\max}, i = 1, 2, \dots, M
 \end{aligned} \tag{2}$$

223

224 where the set of the constraint functions do not allow the “toe” of the interface
 225 x^{toe} to reach the location of pumping wells (Mantoglou et al. 2004). The variable
 226 x_i^{toe} is the horizontal distance of the toe from the coast, as a function of the
 227 pumping rates. In this study, the evolutionary annealing-simplex (EAS) algorithm
 228 (Efstratiadis and Koutsoyiannis 2002) was used to solve the optimization
 229 problems defined in (1) and (2). To apply heuristic optimization, the nonlinear
 230 constraints are embedded in the objective function using penalty terms. Here, the
 231 objective function is penalized according to the following formulation for the
 232 VDST model (Christelis et al. 2017):

233

$$234 \min f(Q) = \begin{cases} -\sum_{i=1}^M Q_i, & \text{if } \forall i = 1, 2, \dots, M; x_i^{cmax}(Q_1, Q_2, \dots, Q_M) \leq xw_i \\ M_v \sum_{i=1}^M \left[\max((x_i^{cmax} - xw_i), 0) \right]^2, & \text{if } \exists i = 1, 2, \dots, M; x_i^{cmax}(Q_1, Q_2, \dots, Q_M) > xw_i \end{cases}$$

235 (3)

236

237 where M_v represents the number of pumping wells that the constraint is violated.

238 A similar formulation is defined for the sharp interface model:

239

$$240 \min f(Q) = \begin{cases} -\sum_{i=1}^M Q_i, & \text{if } \forall i = 1, 2, \dots, M; x_i^{toe}(Q_1, Q_2, \dots, Q_M) < xw_i \\ M_v \sum_{i=1}^M \left[\max((x_i^{toe} - xw_i), 0) \right]^2, & \text{if } \exists i = 1, 2, \dots, M; x_i^{toe}(Q_1, Q_2, \dots, Q_M) \geq xw_i \end{cases}$$

241 (4)

242

243 The few parameters that must be initially set for the EAS algorithm were
 244 defined according to Efstratiadis and Koutsoyiannis (2002) and Tsoukalas et al.
 245 (2016). Thus, the initial population size is set to $n_{pop} = 8M$, the two annealing

246 schedule control parameters to $\lambda p = 0.95$ and $\psi = 2$, the mutation probability is
247 set to $mp = 0.1$ and the convergence criterion to $\varepsilon = 10^{-4}$. For all optimization
248 frameworks the termination criteria are met if the convergence criterion ε equals
249 its pre-set value or the number of maximum objective function evaluations equal
250 $n_{\max} = 100n_{pop}$.

251

252 3. Development of the SBO frameworks

253 3.1 The conventional approach

254 As mentioned in the introduction section there are various surrogate models that
255 can be employed for SBO. Here, cubic radial basis function (RBF) models are
256 utilized. RBF models have been successfully applied in several SBO studies (e.g.
257 Mugunthan et al. 2005; Sun et al. 2011; Tsoukalas et al. 2016; Christelis et al.
258 2017). The training time of cubic RBF surrogate models has a low computational
259 cost which is desirable for the development of a SBO framework. In addition,
260 RBF models are interpolating surrogates which means that they pass through all
261 training data, a favourable feature for approximating the deterministic computer
262 outputs produced in the present work.

263 For convenience, let Q be the decision vector of pumping rates
264 $Q = (Q_1, Q_2, \dots, Q_M)$ and $x_i^{c\max}(Q)$ the scalar response for the i th pumping well as
265 calculated by the VDST simulation. It is noted that the number of the constraint
266 functions equals the number of pumping wells. Therefore, a unique RBF model is
267 constructed for each one of the pumping wells. A Latin Hypercube Sampling
268 (LHS) design was utilized to uniformly sample the decision vector space, evaluate

269 the VDST model and create an initial set of m training patterns for each RBF
 270 model. The set of the decision vectors $Q^{(1)}, Q^{(2)}, \dots, Q^{(m)} \in R^M$ obtained from the
 271 LHS design and the values $x_i^{c\max}(Q^{(1)}), x_i^{c\max}(Q^{(2)}), \dots, x_i^{c\max}(Q^{(m)}), i = 1, \dots, M$
 272 obtained from the VDST model, define a cubic RBF model, augmented with a
 273 linear polynomial tail, of the following form (Powell, 1992):

$$274 \quad S_m(Q) = \sum_{k=1}^m \lambda_k \phi(\|Q - Q^{(k)}\|) + p(Q) \quad (5)$$

275
 276 Here, the cubic form is applied, where $\phi(r) = r^3$, $\lambda_1, \dots, \lambda_m \in R$ are coefficients to
 277 be determined, and $p(Q)$ is a linear polynomial whose coefficients also need to
 278 be determined. To obtain the coefficients in the above cubic RBF model the
 279 matrix $\Phi \in R^{M \times M}$ is defined where $\Phi_{k,l} = \phi(\|Q^{(k)} - Q^{(l)}\|)$ and the matrix
 280 $P \in R^{m \times (M+1)}$ whose i th row is $\left[1, (Q^{(i)})^T\right]$. The vector
 281 $x_i^{VDST} = \left[x_i^{c\max}(Q^{(1)}), x_i^{c\max}(Q^{(2)}), \dots, x_i^{c\max}(Q^{(m)})\right]^T$ is also defined. The vector of
 282 coefficients $\lambda = [\lambda_1, \dots, \lambda_m]^T$ for the RBF part and the coefficients
 283 $c = [c_0, c_1, \dots, c_M]^T$ for the polynomial part are obtained by solving the following
 284 system of linear equations:
 285

$$286 \quad \begin{pmatrix} \Phi & P \\ P^T & 0 \end{pmatrix} \begin{pmatrix} \lambda \\ c \end{pmatrix} = \begin{pmatrix} x_i^{VDST} \\ 0 \end{pmatrix} \quad (6)$$

288

289 In the present study, new training points are added to the initial sampling plan
290 by evaluating the VDST model whenever the surrogate models find a new better
291 solution during the optimization algorithm operations. Whereas this is not
292 considered as a global SBO approach, it can efficiently locate near global optimal
293 solutions and it has been successfully applied in previous single-objective
294 pumping optimization studies of coastal aquifers (Kourakos and Mantoglou 2009).
295 It is possible, particularly during the first few iterations of the EAS algorithm, that
296 the surrogate models will incorrectly predict that $x_i^{c\max}(Q) < x_{init}^{c\max}$, where $x_{init}^{c\max}$ is
297 obtained from the initial simulation with the VDST model without pumping. This
298 could be avoided in a certain degree if we add more training points in the initial
299 sampling design. However here, it was used as an additional model-based
300 criterion to retrain the RBF models during optimization. A summary of the
301 adaptive SBO framework is given below:

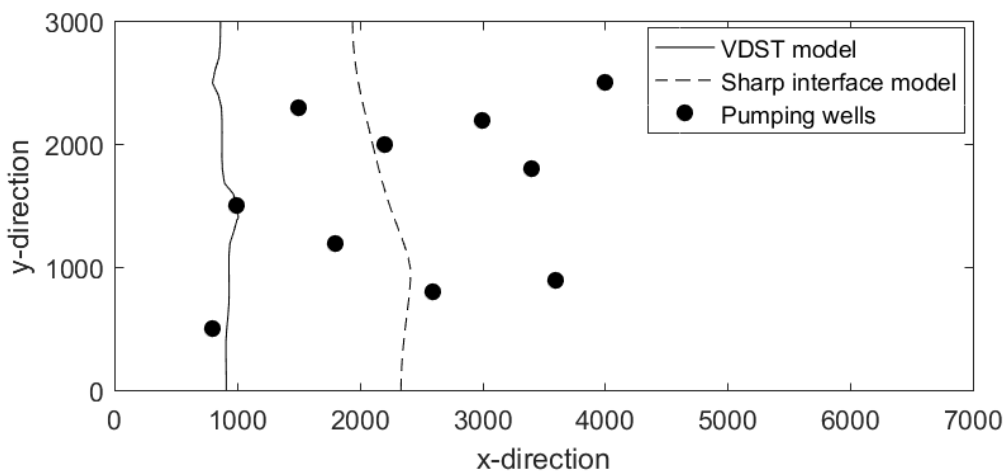
302

- 303 1. Use LHS design to provide the initial m training points $Q^{(1)}, Q^{(2)}, \dots, Q^{(m)}$ and
304 get $x_i^{c\max}(Q^{(1)}), x_i^{c\max}(Q^{(2)}), \dots, x_i^{c\max}(Q^{(m)}), i = 1, \dots, M$ through m VDST
305 simulations.
- 306 2. Construct M RBF models and create an external archive of training patterns.
- 307 3. Run EAS algorithm based on the RBF models and if during optimization a
308 better optimum is found or any ith RBF model prediction is
309 $x_i^{c\max}(Q) < x_{init}^{c\max}$ do the following:
 - 310 a) Re-evaluate the current best decision vector with the VDST model.
 - 311 b) Replace the objective function value with the VDST solution.

- 312 c) Store the new input-output data to the archive and re-train the surrogate
313 models.
314 4. Are stopping criteria for EAS algorithm met? If yes, return final solution, else
315 go to step 3.

316 3.2 The variable-fidelity approach

317 Previous seawater intrusion studies have demonstrated that the sharp interface
318 model utilized here, provides conservative estimations of the optimal pumping
319 rates compared to the VDST model (Pool and Carrera 2011; Kopsiaftis et al.
320 2017). An example is shown in Figure 1 for a specific input Q where the sharp
321 interface model output shows a more severe landward advancement of the
322 seawater wedge.



323

324 **Figure 1.** Advancement of seawater intrusion as simulated by the VDST and the
325 sharp interface model for the same set of pumping rates.

326 In a previous study, Pool and Carrera (2011) developed an empirical
327 correction for the sharp interface model to better match the maximum pumping
328 rates calculated from the VDST models. Practically, a modified density ratio for
329 the sharp interface model of Strack (1976) is calculated based on the aquifer depth

330 B and the transverse dispersivity value α_T defined in the VDST model as follows
331 (see Pool and Carrera, 2011):

332

$$333 \quad \varepsilon^* = \varepsilon \left[1 - \left(\frac{\alpha_T}{B} \right)^{1/6} \right] \quad (7)$$

334

335 where ε is the saltwater-freshwater density ratio defined as $\varepsilon = (\rho_s - \rho_f) / \rho_f$,
336 with ρ_s being the saltwater density and ρ_f the freshwater density. Lu and Werner
337 (2013) proposed that the exponent in equation (7) could be changed to 1/4.
338 However, as it is discussed in Christelis and Mantoglou (2016b) different
339 pumping stresses may require different modifications of the density ratio to
340 achieve a better match for the two models in a pumping optimization problem.
341 Here, for comparison purposes, the variable-fidelity optimization framework is
342 also implemented using the sharp interface model corrected by the different values
343 of the density ratio proposed in Pool and Carrera (2011) and Lu and Werner
344 (2013). Furthermore, all 3 sharp interface models considered here, are also utilized
345 to formulate an ensemble surrogate where each of the sharp interface model
346 response is given an equal weight. This is to investigate if the combination of the
347 variable-fidelity data with a simple averaging approach can improve the
348 exploration of the optimal search space.

349 Several response correction techniques have been suggested in the literature
350 such as multiplicative or additive formulations (Leary et al. 2003). A simple
351 correction process can be modeled by any approximation model (e.g. radial basis
352 functions, kriging, etc.) which is fitted, for example, to the ratio R_{HF} / R_{LF} or to the

353 difference $R_{HF} - R_{LF}$, with R_{HF} and R_{LF} being the high-fidelity and lower-fidelity
354 model responses, respectively (Forrester et al. 2008). Let $x_i^{toe}(Q)$ be the scalar
355 response for the i th pumping well as calculated by the sharp interface simulation.
356 The initial training points $Q^{(1)}, Q^{(2)}, \dots, Q^{(m)} \in R^M$ produced by the LHS design are
357 also used here to obtain $x_i^{toe}(Q^{(1)}), x_i^{toe}(Q^{(2)}), \dots, x_i^{toe}(Q^{(m)}), i = 1, \dots, M$ through
358 simulation with the sharp interface model. The corresponding values from the
359 VDST model are $x_i^{cmax}(Q^{(1)}), x_i^{cmax}(Q^{(2)}), \dots, x_i^{cmax}(Q^{(m)}), i = 1, \dots, M$. A cubic RBF
360 model is then trained to approximate a simple multiplicative formulation of the
361 form $x_i^{cmax}(Q)/x_i^{toe}(Q)$ adopted for each one of the pumping wells. Thus, the
362 surrogate model predicts the $x_i^{cmax}(Q)$ value for the i th pumping well based on
363 the following correction:

364

$$365 \quad \hat{x}_i^{cmax}(Q) = x_i^{toe}(Q)S(Q) \quad (8)$$

366

367 Therefore, the sharp interface model corrected by the RBF model is the surrogate
368 model for the VDST model. For each pumping well, a unique RBF model S is
369 constructed. This scaling model between the lower-fidelity and the high-fidelity
370 data, may be reconstructed during optimization, if the evaluation with the high-
371 fidelity model indicates a poor performance of the corrected LF model (Thokala
372 and Martins, 2007). A similar adaptive SBO framework with the conventional
373 approach is also used for the variable-fidelity optimization strategy:

374

- 375 1. Use LHS design to provide the initial m training points $Q^{(1)}, Q^{(2)}, \dots, Q^{(m)}$ and
376 get $x_i^{c\max}(Q^{(1)}), x_i^{c\max}(Q^{(2)}), \dots, x_i^{c\max}(Q^{(m)}), i = 1, \dots, M$ through m high-fidelity
377 simulations and $x_i^{toe}(Q^{(1)}), x_i^{toe}(Q^{(2)}), \dots, x_i^{toe}(Q^{(m)}), i = 1, \dots, M$ through m
378 lower-fidelity simulations.
- 379 2. Create an external archive of training patterns of the above high-fidelity and
380 lower-fidelity data and train M RBF models to learn the ratio
381 $x_i^{c\max}(Q)/x_i^{toe}(Q)$.
- 382 3. Run EAS algorithm based on the surrogate model described in equation (8).
- 383 4. If during optimization a better optimum is found or the i th surrogate model
384 prediction is $x_i^{c\max}(Q) < x_{init}^{c\max}$ do the following:
- 385 a. Re-evaluate the current decision vector with the VDST model.
- 386 b. Replace the objective function value with the VDST solution.
- 387 c. Store the new input-output data to the archive and re-train the
388 surrogate models.
- 389 5. Are stopping criteria for EAS algorithm met? If yes, return final solution, else
390 go to step 3.

391 **4. Results and discussion**

392 Since EAS is a probabilistic optimization method, a set of 30 independent
393 optimization runs was used for each SBO approach to build more confidence
394 among the optimal results. Furthermore, for each optimization run a different
395 initial training set was produced with the VDST model and it was applied as initial
396 population for the EAS algorithm. Thus, for each run, all surrogate models were
397 trained under the same sampling design and the optimal solutions were also based

398 on the same initial population to ensure a fair comparison among them. To handle
399 the computational burden, a single run was executed for each of the direct
400 optimization with the VDST and the sharp interface models. This is also justified
401 by the robust performance of EAS in previous coastal aquifer management studies
402 with these models (Christelis and Mantoglou 2016a). For convenience, the
403 optimization frameworks are henceforth referred with their abbreviated names as
404 follows:

405

- 406 1. EAS-HF: direct optimization using the high-fidelity VDST model.
- 407 2. EAS-LF: direct optimization using the sharp interface model
- 408 3. EAS-LF-PC: direct optimization using the sharp interface model with
409 density ratio corrected as in Pool and Carrera (2011).
- 410 4. EAS-LF-LW: direct optimization using the sharp interface model with
411 density ratio corrected as in Lu and Werner (2013).
- 412 5. EAS-RBF: Conventional SBO using the RBF models.
- 413 6. EAS-VF: Variable-fidelity SBO using the sharp interface model.
- 414 7. EAS-VF-PC: Variable-fidelity SBO using the sharp interface model with
415 density ratio corrected as in Pool and Carrera (2011).
- 416 8. EAS-VF-LW: Variable-fidelity SBO using the sharp interface model with
417 density ratio corrected as in Lu and Werner (2013).
- 418 9. EAS-VF-ENS: Variable-fidelity SBO with all 3 sharp interface models
419 forming an ensemble in a simple averaging approach.

420

421 Table 2 presents the summary statistics of the SBO runs along with the results
422 from direct optimization with the seawater intrusion models.

423 **Table 2.** Summary statistics comparisons among the optimization frameworks. The best SBO
 424 performance is highlighted while the high-fidelity solution from the VDST model is underlined.

	Best (m^3/day)	Worst (m^3/day)	Median (m^3/day)	CPU time (hr) (average*)
EAS-HF	<u>4871.6</u>	n/a	n/a	44.8
EAS-LF	2683.9	n/a	n/a	0.8
EAS-LF-PC	4810.3**	n/a	n/a	0.8
EAS-LF-LW	4724.4**	n/a	n/a	0.8
EAS-RBF	4856.8	4378.1	4703.6	1.64
EAS-VF	4868.3	4372.3	4697.4	2.36
EAS-VF-PC	4768.2	4585.9	4720	2.36
EAS-VF-LW	4780.1	4538.4	4697.6	2.36
EAS-VF-ENS	4796.9	4577.1	4731.2	2.66

425 n/a: not applicable

426 *: only for the SBO frameworks

427 **: not a feasible solution after evaluation with the VDST model

428

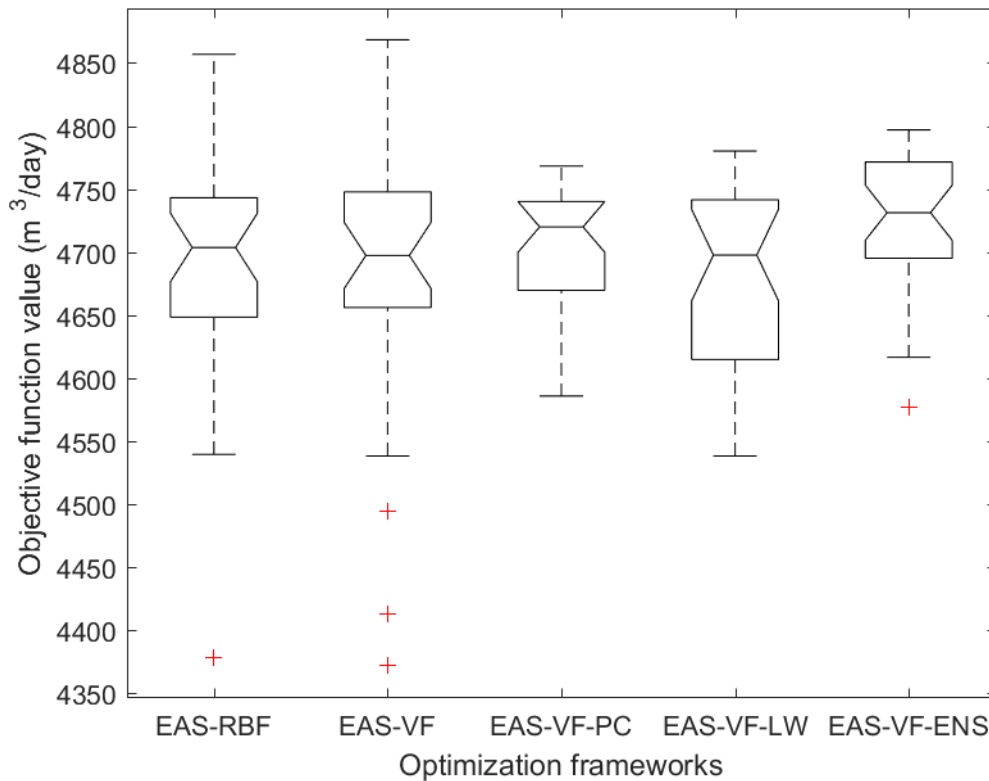
429 As expected, EAS-LF produced the lowest best objective function value, since the
 430 sharp interface model tends to overestimate seawater intrusion and therefore lower

431 maximum pumping rates are calculated (Pool and Carrera, 2011). On the contrary,
432 EAS-LF-PC and EAS-LF-LW provided higher optimal solutions than EAS-LF
433 since the modification of the density ratio allows for larger groundwater
434 extraction. Note that the optimal solutions obtained from the sharp interface
435 models were evaluated using the VDST model. This is because EAS-LF, EAS-
436 LF-PC and EAS-LF-LW frameworks do not involve any high-fidelity VDST runs.
437 Thus, their optimal solutions were evaluated with the VDST model to check if
438 they are feasible based on the set of constraints which are defined on the VDST
439 model. The EAS-LF solutions were feasible but the EAS-LF-PC and EAS-LF-LW
440 violated the constraints for the VDST model. Nevertheless, the above results do
441 not conclude that EAS-LF-PC or EAS-LF-LW optimization would generally fail
442 to provide feasible optimal solutions. The corrections proposed in Pool and
443 Carrera (2011) and Lu and Werner (2013) constitute one-off corrections of the
444 sharp interface model and the latter may approximate different parts of the
445 dispersive zone of the VDST model depending also on the hydraulic parameter
446 sets in both models. Therefore, other salinity levels defined in the VDST-based
447 optimization may be satisfied by the solutions produced from EAS-LF-PC or
448 EAS-LF-LW. It cannot be ignored that these approaches can potentially provide
449 information for regions with good local optima for the VDST model.

450 As also shown in Table 2, EAS-RBF was the most computationally efficient
451 method among the SBO frameworks, requiring less than an hour to converge. It
452 also came second on providing the best objective function value after EAS-VF.
453 The variable-fidelity methods in general, required approximately 30% more
454 computational time to converge than the conventional EAS-RBF approach. The
455 ensemble approach (EAS-VF-ENS) provided the highest median but also had the

456 largest computational cost among the SBO methods. Figure 2 presents the
457 distribution of the optimal solutions via box plot visualization for a more detailed
458 comparison of the SBO frameworks.

459



460

461 **Figure 2.** Performance of the SBO frameworks based on boxplots

462

463 As demonstrated the interval endpoints of the boxplot notches appear to overlap
464 which implies that the medians of the SBO frameworks probably do not exhibit
465 any statistically significant difference. Although the SBO sample runs are limited
466 due to computational restrictions, a one-way analysis of variance (ANOVA) test
467 also provided a p-value of 0.18 which increases the belief that for the case studied
468 here the medians are not significantly different at a 5% significance level. It is
469 interesting to see the average percentage of the successful predictions of feasible
470 solutions with the surrogate models as these were evaluated by the VDST model

471 during the operations of the optimization algorithm. That is, how many of the
 472 constraint function predictions from the surrogates were feasible whenever the
 473 VDST was called by the SBO algorithm to evaluate the current solution. The
 474 EAS-VF-ENS has a higher percentage than the other SBO methods while the
 475 other variable-fidelity methods (EAS-VF, EAS-VF-PC and EAS-VF-LW)
 476 demonstrate similar performance but not as good as the conventional EAS-RBF
 477 approach. Given, the similar statistical performance of all the SBO frameworks it
 478 appears that even the less accurate constructed surrogate models can still drive the
 479 optimization algorithm to good optimal solutions.

480 **Table 3.** Successful surrogate model predictions of feasible solutions based on the VDST model
 481 evaluation during the optimization operations.

	EAS-RBF	EAS-VF	EAS-VF-PC	EAS-VF-LW	EAS-VF-ENS
Percentage of feasible surrogate model predictions (average)	60.19	57.26	57.89	57.30	61.71

482

483 **5. Conclusions**

484 The problem of pumping optimization of coastal aquifers was solved considering
 485 direct optimization, as well as, SBO methods to reduce the computational cost
 486 derived from variable density and salt transport simulations. The SBO methods
 487 were developed using an adaptive framework by embedding the surrogate model
 488 update process in the operations of an evolutionary optimization algorithm. A

489 conventional and a variable-fidelity surrogate model approach were employed.
490 The objective was to identify whether a variable-fidelity approach which utilizes a
491 simple scaling function that corrects the lower-fidelity models can outperform the
492 conventional SBO and provide good approximations to the direct high-fidelity
493 optimization. The variable-fidelity method was developed using the sharp
494 interface assumption and the single-potential formulation of Strack (1976), as well
495 as variations of this model based on recent proposed correction factors. In
496 addition, an ensemble surrogate model, based on a simple averaging approach,
497 was constructed by using all the variations of the sharp interface model.

498 Results demonstrated that the SBO approaches performed equally well and
499 found optimal solutions close to those obtained from the direct optimization with
500 the high-fidelity VDST model. The computational gains by applying the SBO
501 methods were above 90% of the computational time from the VDST-based
502 optimization. Although the variable-fidelity approach provided the best optimal
503 solution and the highest median, it also added computational cost. Furthermore,
504 the overall sample statistics implied that there wasn't a statistically significant
505 difference among the medians of the SBO methods. The combination of all sharp
506 interface models to form an ensemble surrogate model reduced the spread of the
507 solutions and provided the highest median but failed to find the best objective
508 function value among the SBO frameworks. The overall understanding is that
509 given the lower computational cost of the conventional SBO approach, the
510 variable-fidelity method followed in this study couldn't provide strong evidence
511 than can perform better based on the derived sample statistics.

512 However, the results here are limited to the coastal aquifer model settings that
513 were adopted in this study. It is of practical interest to investigate if variable-

514 fidelity methods can provide an effective alternative to SBO for coastal aquifer
515 management studies by testing other model settings and different correction and
516 enhancement techniques of lower-fidelity seawater intrusion models. Future work
517 will focus on utilizing other levels of fidelity apart from the sharp interface
518 assumption, as well as investigating the construction of efficient surrogate
519 ensembles based on models of variable-fidelity.

520

521 **References**

- 522 Alexandrov NM, Lewis RM, Gumbert CR, Green LL, Newman PA (2001) Approximation and
523 model management in aerodynamic optimization with variable-fidelity models. *J Aircraft*
524 38(6):1093-1101
- 525 Asher MJ, Croke BFW, Jakeman AJ, Peeters LJM (2015) A review of surrogate models and their
526 application to groundwater modeling. *Water Resour Res* 51(8): 5957-5973
- 527 Ataie-Ashtiani B, Ketabchi H, Rajabi MM (2013) Optimal management of a freshwater lens in a
528 small island using surrogate models and evolutionary algorithms. *J Hydrol Eng* 19(2):339-354
- 529 Bakker M (2003) A Dupuit formulation for modeling seawater intrusion in regional aquifer
530 systems. *Water Resour Res* 39(5)
- 531 Bandler JW, Biernacki RM, Chen SH, Grobelny PA, Hemmers RH (1994) Space mapping
532 technique for electromagnetic optimization. *IEEE T Microw Theory* 42(12):2536-2544
- 533 Bandler JW, Cheng QS, Nikolova NK, Ismail MA (2004) Implicit space mapping optimization
534 exploiting preassigned parameters. *IEEE T Microw Theory* 52(1): 378-385.
- 535 Christelis V, Mantoglou A (2016a) Pumping optimization of coastal aquifers assisted by adaptive
536 metamodelling methods and radial basis functions. *Water Resour Manage* 30(15):5845-5859
- 537 Christelis V, Mantoglou A (2016b) Coastal aquifer management based on the joint use of density-
538 dependent and sharp interface models. *Water Resour Manage* 30(2):861-876
- 539 Christelis V, Regis RG, Mantoglou A (2017) Surrogate-based pumping optimization of coastal
540 aquifers under limited computational budgets. *J Hydroinform* 20(1):164-176

541 Dokou Z, Karatzas GP (2012) Saltwater intrusion estimation in a karstified coastal system using
542 density-dependent modeling and comparison with the sharp-interface approach. *Hydrol Sci J*
543 57(5):985–999

544 Essaid HI (1986) A multilayered sharp interface model of coupled freshwater and saltwater flow in
545 coastal systems: Model development and application. *Water Resour Res* 26(7):1431-1454

546 Park C, Haftka RT, Kim NH (2017) Remarks on multi-fidelity surrogates. *Struct Multidiscip Optim*
547 55(3):1029-1050.

548 Forrester AIJ, Sóbester A, Keane AJ (2008) *Engineering design via surrogate modelling-A practical*
549 *guide*. Wiley, New York

550 Forrester AIJ, Keane AJ (2009) Recent advances in surrogate-based optimization. *Prog Aerosp Sci*
551 49:50-79

552 Gano S, Sanders B, Renaud J (2004) Variable fidelity optimization using a kriging-based scaling
553 function. In 10th AIAA/ISSMO Multidisciplinary analysis and optimization conference (p. 4460).

554 Graf T, Therrien R (2005) Variable-density groundwater flow and solute transport in porous media
555 containing nonuniform discrete fractures. *Adv Water Resour* 28:1351-1367

556 Huang PS, Chiu YC (2018) A Simulation-Optimization Model for Seawater Intrusion Management
557 at Pingtung Coastal Area, Taiwan. *Water* 10(3):251.

558 Hussain MS, Javadi AA, Ahangar-Asr A, Farmani R (2015) A surrogate model for simulation–
559 optimization of aquifer systems subjected to seawater intrusion. *J Hydrol* 523:542-554

560 Karatzas GP, Dokou Z (2015) Optimal management of saltwater intrusion in the coastal aquifer of
561 Malia, Crete (Greece) using particle swarm optimization. *Hydrogeol J* doi: 10.1007/s10040-015-
562 1286-6

563 Kennedy MC, O'Hagan A (2000) Predicting the output from a complex computer code when fast
564 approximations are available. *Biometrika* 87(1):1-13

565 Kerrou J, Renard P, Cornaton F, Perrochet P (2013) Stochastic forecasts of seawater intrusion
566 towards sustainable groundwater management: application to the Korba aquifer (Tunisia).
567 *Hydrogeol J* 21(2):425-440

568 Kopsiaftis G, Christelis V, Mantoglou A (2017) Pumping optimization in coastal aquifers:
569 Comparison of sharp interface and density dependent models. *European Water*, 57: 443-449

570 Kourakos G, Mantoglou A (2009) Pumping optimization of coastal aquifers based on evolutionary
571 algorithms and surrogate modular neural network models. *Adv Water Resour* 32(4): 507-521

572 Koussis AD, Mazi K, Destouni G (2012) Analytical single-potential, sharp-interface solutions for
573 regional seawater intrusion in sloping unconfined coastal aquifers, with pumping and recharge. *J*
574 *Hydrol* 416:1-11

575 Koziel S, Bandler JW, Madsen K (2006) A space-mapping framework for engineering
576 optimization—Theory and implementation. *IEEE T Micro Theory Techniques*, 54(10):3721-3730

577 Koziel S, Leifsson L (2016) *Simulation-Driven Design by Knowledge-Based Response Correction*
578 *Techniques*. New York, Springer

579 Lal A, Datta B (2018) Development and Implementation of Support Vector Machine Regression
580 Surrogate Models for Predicting Groundwater Pumping-Induced Saltwater Intrusion into Coastal
581 Aquifers. *Water Resour Manage* 32(7):2405-2419

582 Leary SJ, Bhaskar A, Keane AJ (2003) A knowledge-based approach to response surface modelling
583 in multifidelity optimization. *J Global Optim* 26(3):297-319

584 Lu C, Werner AD (2013) Timescales of seawater intrusion and retreat. *Adv. Water Resour.* 59:39-
585 51.

586 Mahmoodzadeh D, Ketabchi H, Ataie-Ashtiani B, Simmons CT (2014) Conceptualization of a fresh
587 groundwater lens influenced by climate change: A modeling study of an arid-region island in the
588 Persian Gulf. Iran. *J Hydrol* 519: 399-413

589 Mantoglou A, Papantoniou M, Giannouloupoulos P (2004) Management of coastal aquifers based on
590 nonlinear optimization and evolutionary algorithms. *J Hydrol* 297(1–4):209–228

591 Mugunthan P, Shoemaker CA, Regis RG (2005) Comparison of function approximation, heuristic,
592 and derivative- based methods for automatic calibration of computationally expensive groundwater
593 bioremediation models. *Water Resour Res* 41(11)

594 Papadopoulou MP, Nikolos IK, Karatzas GP (2010) Computational benefits using artificial
595 intelligent methodologies for the solution of an environmental design problem: saltwater intrusion.
596 *Water Sci Technol* 62(7):1479-1490

597 Petalas C, Pisinaras V, Gemitzi A, Tsihrintzis VA, Ouzounis K (2007) Current conditions of
598 saltwater intrusion in the coastal Rhodope aquifer system, northeastern Greece. *Desalination*
599 237:22-41

600 Pool M, Carrera J (2011) A correction factor to account for mixing in Ghyben-Herzberg and critical
601 pumping rate approximations of seawater intrusion in coastal aquifers. *Water Resour Res*
602 doi:10.1029/2010WR010256

603 Powell MJD (1992) The theory of Radial Basis Function Approximation in 1990, in: Light, W.
604 (ed.), *Advances in Numerical Analysis, Volume 2: Wavelets, Subdivision Algorithms and Radial*
605 *Basis Functions*. pp. 105–210, Oxford University Press

606 Rajabi MM, Ketabchi H (2017) Uncertainty-based simulation-optimization using Gaussian process
607 emulation: Application to coastal groundwater management. *J Hydrol* 555:518-534

608 Razavi S, Tolson BA, Burn DH (2012a) Review of surrogate modeling in water resources. *Water*
609 *Resour Res* 48(7)

610 Regis RG, Shoemaker CA (2005) Constrained global optimization of expensive black box functions
611 using radial basis functions. *J Global Optim* 31(1):153-171.

612 Regis RG (2011) Stochastic radial basis function algorithms for large-scale optimization involving
613 expensive black-box objective and constraint functions. *Comput Oper Res* 38:837-853

614 Robinson T, Willcox K, Eldred M, Haimes R (2006) Multifidelity optimization for variable-
615 complexity design. In 11th AIAA/ISSMO multidisciplinary analysis and optimization conference
616 (p. 7114)

617 Roy DK, Datta B (2017a) Fuzzy C-Mean Clustering Based Inference System for Saltwater
618 Intrusion Processes Prediction in Coastal Aquifers. *Water Resour Manage* 31(1):355-376

619 Roy DK, Datta B (2017b) Multivariate Adaptive Regression Spline Ensembles for Management of
620 Multilayered Coastal Aquifers. *J Hydrol Eng* 22(9):04017031

621 Song J, Yang Y, Wu J, Wu J, Sun X, Lin J (2018) Adaptive surrogate model based multiobjective
622 optimization for coastal aquifer management. *J Hydrol* 561:98-111

623 Sreekanth J, Datta B (2011) Comparative evaluation of Genetic Programming and Neural Network
624 as potential surrogate models for coastal aquifer management. *Water Resour Manage* 25:3201-3218

625 Sreekanth J, Datta B (2015) Review: Simulation-optimization models for the management and
626 monitoring of coastal aquifers. *Hydrogeol J* doi:10.1007/s10040-015-1272-z

627 Strack ODL (1976) A single-potential solution for regional interface problems in coastal aquifers.
628 *Water Resour Res* 12(6):1165–1174

629 Sun G, Li G, Gong Z, He G, Li Q (2011) Radial basis functional model for multi-objective sheet
630 metal forming optimization. *Eng Optim* 43(12):1351-1366

631 Therrien R, McLaren RG, Sudicky EA, Panday SM (2006) HydroGeoSphere-A three-dimensional
632 numerical model describing fully-integrated subsurface and surface flow and solute transport.
633 Groundwater Simulations Group, University of Waterloo, Canada, draft ed. 2006

634 Thokala P, Martins JR (2007) Variable-complexity optimization applied to airfoil design. *Eng*
635 *Optimiz* 39(3):271-286

636 Tsoukalas I, Kossieris P, Efstratiadis A, Makropoulos C (2016) Surrogate-enhanced evolutionary
637 annealing simplex algorithm for effective and efficient optimization of water resources problems on
638 a budget. *Environ Modell Softw* 77: 122-142

639 Werner AD, Bakker M, Post VEA, Vandenbohede A, Lu C, Ataie-Ashtiani B, Simmons CT, Barry
640 DA (2013) Seawater intrusion processes, investigation and management: Recent advances and
641 future challenges. *Adv Water Resour* 51:3-26

642 Zhou Q, Shao X, Jiang P, Gao Z, Wang C, Shu L (2016) An active learning metamodeling
643 approach by sequentially exploiting difference information from variable-fidelity models. *Adv Eng*
644 *Inform*, 30(3):283-297

645 Zhou Q, Wang Y, Jiang P, Shao X, Choi SK, Hu J, Cao L, Meng X (2017) An active learning radial
646 basis function modeling method based on self-organization maps for simulation-based design
647 problems. *Knowl-Bas Syst*, 131:10-27

648